Electrochimica Acta 134 (2014) 28–34

Contents lists available at ScienceDirect

Electrochimica Acta

journal homepage: www.elsevier.com/locate/electacta

One novel and universal method to prepare transition metal nitrides doped graphene anodes for Li-ion battery

Linfei Lai[a,b,c], Jixin Zhu[d], Baosheng Li[c], Yongda Zhen[b], Zexiang Shen[a], Qingyu Yan[d], Jianyi Lin[c,*]

[a] Division of Physics and Applied Physics, School of Physical and Mathematical Sciences, Nanyang Technological University, Singapore, 637371, Singapore
[b] Institute of Chemical and Engineering Sciences, A*STAR, 1 Pesek Road, Jurong Island, Singapore, 627833, Singapore
[c] Energy Research Institute @ NTU (ERI@N), Singapore, 637141, Singapore
[d] School of Materials Science and Engineering, Nanyang Technological University, 50 Nanyang Avenue, Singapore, 639798, Singapore

ARTICLE INFO

Article history:
Received 25 November 2013
Received in revised form 10 April 2014
Accepted 10 April 2014
Available online 21 April 2014

Keywords:
Graphene oxide
Transition metal nitride
Lithium ion battery

ABSTRACT

Transition metal nitrides (TMN)/N modified graphene (N-rG-O) composites are prepared by annealing of $Metal^{n+}$-EN (EN: ethylene diamine) chelate and G-O composite. Li-storage and cycling behavior of TMN/N-rG-O composite have been evaluated by galvanostatic discharge-charge and cyclic voltammetry in coin cells with Li-metal as counter electrode. FeN/N-rG-O, CoN/N-rG-O, FeCoN/N-rG-O, NiN/N-rG-O are prepared using this method, and all have shown pronounced cyclability and considerable high capacity value. Even a low loading of TMN (12.5% ±2.0%) on graphene can significantly improve the Li-ion storage capacity of graphene. For example, FeN/N-rG-O with FeN weight ratio of only 12.5% has an initial reversible capacity of 665 ± 10 $mAhg^{-1}$ at a current density of 50 $mA\,g^{-1}$, and the capacity value further increase consistently to 698 ±10 $mAhg^{-1}$ after 50 cycles. The excellent cyclability, low charge/discharge potentials (<1.5 V), high reversible capacity values of TMN/N-RG-O indicate they are prospective anodes for Li-ion batteries.

1. Introduction

Among various energy conversion/storage systems proposed over the two last centuries, electrochemical storage and more specifically battery exhibiting improved energy densities and lifetimes is promising, [1,2] but research aiming at meet commercial application requirements is still in imperious need. Graphite is conventional anode material for lithium-ion batteries (LIBs) with high columbic efficiency (> 85%) and excellent cycle performance. However, the theoretical lithium storage capacity of graphite is only 372 mAh g^{-1} by forming intercalation compounds (LiC_6). [3] Metals and semimetals can electrochemically form alloys with lithium with large capacity achieved from alloying reactions (Sn + 4.4 Li ↔ $Li_{4.4}Sn$). However the huge volume change associate to the de-alloying process introduces large strain in metals/semimetals, which subsequently cause their structural deformation, and irreversible capacity loss of the electrodes. Metal oxides, such as Co_3O_4, [4,5] SnO_2, [6,7] Fe_xO_y, [8,9] which have been extensively studied as anode for Li-ion batteries, can reversibly react with Li through conversion reaction (eg., Fe_2O_3 + 6Li ↔ 2Fe +3Li_2O). These metal oxides could deliver capacity values two or three times larger than that of graphite. However, the practical utilization of these materials needs to apply carbon coating, carbon additives or reduce the size of metal oxides to nano scale in order to reduce the capacity loss from structural deformation during cycling. [10] The structural and component control of metal oxides composite [11] would somewhat alleviate their capacity loss during cycling, but their performance is still far from satisfying.

Due to the low conversion reaction potentials of transition metal nitrides (TMNs) with Li, [3] there has been surge of interest in developing advanced materials of twofold metal nitrides as LIBs negative electrodes, such as SnN, [12] CrN, VN, [13] Mn_3N_2, [14] and NiN, [15] etc. The electrochemical behavior of these metal nitrides (such as CoN, [16] FeN, [17] CrN, [18,19] VN [13]) with lithium as anode materials have been widely investigated, which can be indexed to conversion reaction mechanism. Lithiated transition metal nitrides (LiTMNs), such as Li_3FeN_2 and $Li_{3-x}Co_xN$, which are byproducts of TMN after Li-ion insertion, can store Li ions by intercalation and de-intercalation mechanism in early studies. [14,20,21] These LiTMNs, such as $LiMnN_2$, [22] $Li_{3-x}TM_xN$ (M = Co, Ni), [23] $Li_{2.6}Co_{0.4}N$ [24] have been identified to be the most promising negative electrodes, with reversible capacity between 400 and 760 $mAhg^{-1}$.

* Corresponding author.
E-mail address: lin_jianyi@ices.a-star.edu.sg (J. Lin).

http://dx.doi.org/10.1016/j.electacta.2014.04.073
0013-4686/

TMN also exhibit excellent properties of high melting point and chemically inert behavior, therefore, advantageous for electrode materials to be protected from moist or erosive environments. [17] There have been several reports concerning the preparation and application of TMNs in the past few years, in which magnetron sputtering is commonly used method, [25–27] and nitrogen gas is the metal nitridation source. However, as the inert nature of N_2, the reaction is costly and not suitable for large-scale preparation.

Graphene, a monolayer of carbon has attract numerous interest from fundamental research to practical applications due to its interesting electrical properties, such as high surface area, chemical tolerance and broad electrochemical window. [28,29] It is found that the theoretical specific Li storage capacity for graphene is 744 $mAhg^{-1}$, corresponding to the formation of LiC_3. [30] However, graphene-based all-carbon electrodes are reported to suffer from a low initial coulombic efficiency, and large capacity fade during cycles. Graphene combined with transition metal oxides are reported to exhibit high capacity value, long cycle life, and good rate performance, however, these materials, like graphene/Co_3O_4 [31], and graphene/Fe_2O_3 [32] etc., still have high discharge profile. The high discharge voltage of these transition metal oxides/graphene composites will cause the full cell voltage reduction after matched with suitable cathode materials, and further cause decrease of energy density. Therefore, the combination of graphene with TMNs which has low conversion reaction potentials towards Li would have practical application as Li-ion battery anodes.

In this paper, we report the synthesis of TMNs (FeN, FeCoN, NiN, and CoN)/N-rG-O composite by a simple and universal chemical method. The transition metal chelates (TMN^{n+}-EN) which has–NH_2 functional groups could be easily attached onto O-containing functional groups on G-O surface. The G-O was reduced and doped with N after refluxing with TMN^{n+}-EN/G-O composite and further annealing, while TMN nanoparticles were formed on graphene surface meanwhile. Electrochemical measurements demonstrated that TMN/N-rG-O presented a higher relative specific capacity and excellent cycling stability, compared with rG-O, N-rG-O sheets, indicating its great potential as an anode material for Li-ion batteries.

2. Experimental Section

GO were prepared from natural graphite powder by chemical exfoliation using modified Hummers method. The GO solution with concentration of 2 mg/mL was freeze dried for further use.

Preparation of FeN/N-rG-O: 200 mg of iron acetate was fully dissolved in 125 mL of ethanol before adding 1 mL of ethylenediamine (EN). The solution was stirred for half an hour, creating a Fe-EN complex. 100 mL of 2 mg/mL G-O solution was separately dispersed in 125 mL of ethanol and then added to the Fe-EN complex solution. The combined solution was then refluxed at 100 °C for an hour under ambient pressure and further dried. The remaining dried precipitate was pyrolyzed at 550 and 850 °C for 1 h under 5% NH_3/Ar (120 sccm) protection. The as-obtained powder was then grounded with mortar for 20 mins and treated with 1 M H_2SO_4 at 80 °C for 12 h before being filtered, washed with large amount of DI water and vacuum-dried at 80 °C. The CoN/N-rG-O, NiN/N-rG-O and FeCoN/N-rG-O were prepared in the same procedure but replacing iron acetate with cobalt nitrate, nickel nitrate, or iron acetate and cobalt nitrate mixture (molar ratio of Fe:Co = 1:1), respectively.

Characterization: The morphology and structure of samples were characterized by field-emission scanning electron microscope (FESEM, JEOL JSM-6700F, 15 kV) and high-resolution analytical transmission electron microscopy (TEM) (Model JEM-2010F, JEOL, Tokyo, Japan, 200 kV). The crystal structure of the samples was examined by a Bruker D/MAX 2500 X-ray diffractometer (XRD) with Cu Kα radiation (λ = 1.54056 Å). The XPS was characterized on Kratos Axis Ultra DLD (delay line detector) spectrometer using monochromatic Al Kα (hν =1486.6 eV) X-ray source with resolution of 0.1 eV. The elemental compositions of the TMN/N-rG-O were analyzed on an inductively coupled plasma-optical emission spectrometer (ICP-OES, Varian Vista-MPX CCD Simultaneous ICP-OES). The individual TMN/N-rG-O sample for the analysis was digested using aqua regia and kept in 2% HNO_3.

Electrochemical measurements: For electrochemical measurements, the cells were constructed by using as-prepared metal nitrides as a working electrode and lithium metal at a counter electrode. The working electrodes were prepared by mixing 80 wt % active material (TMN/N-rG-O, N-rG-O or rG-O), 10 wt % acetylene black (Super-P), and 10 wt % polyvinylidene fluoride (PVDF, 5 wt %) binder dissolved in N-methyl-2-pyrrolidinone. After coating the above slurries on Cu foils, the electrodes were dried at 110 °C in vacuum for 2 h to remove the solvent before pressing. Then the electrodes were cut into disks (16 mm in diameter) and dried at 100 °C for 24 h in vacuum. The CR2032 (3 V) coin-type cell were assembled in an Ar-filled glove-box with lithium metal as the counter/reference electrode, Celgard 2400 membrane as separator, and 1 M $LiPF_6$ electrolyte. The electrolyte solution was prepared by dissolving 1 M $LiPF_6$ in a mixture of ethylene carbonate (EC) and dimethyl carbonate (DMC) (EC/DMC, 1:1 v/v). The CV measurements were carried out using a Solartron 1287 electrochemical workstation at a scanning rate of 1 mV s^{-1}. Galvanostatic discharge/charge cycles were tested by LAND CT2001A electrochemical workstation at various current densities of 50∼100 mA g^{-1} between 0.01 and 3 V (*vs* Li^+/Li) at room temperature.

3. Results and Discussion

3.1. Synthesis and Characterization

The growth of TMN requires the presence of active N atoms and metal ions. Ethylene diamine (EN) is a well-known chelating ligand for coordination compound which forms derivatives with carboxylic acid, carbon disulfide, and ketones etc. EN can be easily coordinated with transition metal ions (TMN^{n+}) to form a TMN^{n+}-EN complex. G-O has abundant O-containing functional groups, which is capable of adsorbing TMN^{n+}-EN chelates through electrostatic interaction. After refluxing TMN^{n+}-EN complex and G-O under 110 °C, some of the O-containing functional groups in G-O could be replaced by–NH_2 groups from TMN^{n+}-EN complex with covalent C-N bonds formed between TMN^{n+}-EN and graphene network. As shown in Fig. 1, the TMN^{n+}-EN chelates could be anchored at graphene edges or on the basal plane of graphene layers where located abundant O-containing functional groups. The TMN nanoparticles were formed after TMN^{n+}-EN/G-O composite annealed, while G-O was reduced and doped with N meanwhile. The final product was then soaked by 1 M of H_2SO_4 under 80 °C for 12 h, and then washed by large quantity of water until the pH value of supernatant is around 7.

The composition of the TMN/N-rG-O was confirmed by X-ray diffraction (XRD) pattern as shown in Fig. 2. The FeN/N-rG-O samples prepared in different annealing temperatures (550 and 850 °C) were selected for characterization. Both FeN/N-rG-O 550 and 850 °C show broad peak at 27° suggesting increased interlamellar spacing of N-rG-O compared with that of G-O as reported. [33] For the FeN/N-rG-O annealed under 550 °C, has several sharp peaks correspond to the 104, 110, 024 and 116 faces of Fe_2O_3 (JCPDS: 01-1053), with peak positions well fitted. XRD pattern of FeN/N-rG-O 550 °C indicate the presence of Fe_2O_3 which was coated or enwrapped by graphene layers, and was not completely removed by acid bleaching. According to phase diagrams of Fe-N and

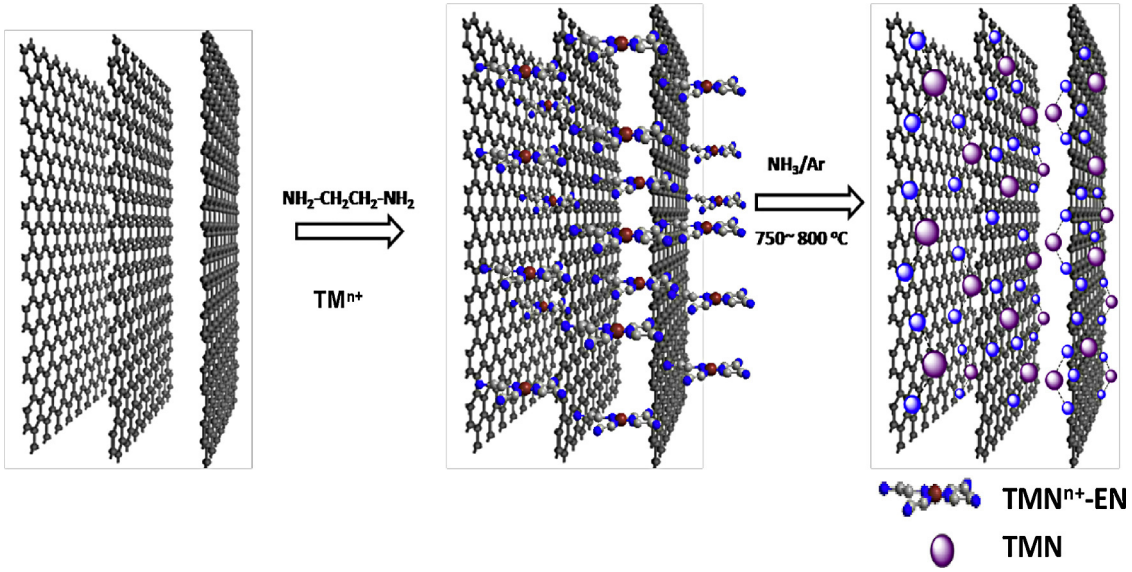

Fig. 1. Schematic illustration for the preparation of TMN/N-rG-O.

Fe-C, [34] nitrogen can dissolve rapidly into iron at ~590 °C. [35] Therefore, pyrolysis of FeN/N-rG-O chelates above temperature 590 °C is favorable to obtain metal nitrides. FeN/N-rG-O has intense diffraction peak at 43.49° associate with (101) face of Fe_3N (JCPDS: 049-1662).

SEM images indicate both particles (~5-50 nm) and tube/rod like materials were distributed on graphene surface. The particles with size larger than 50 nm has vacant carbon shell as observed by TEM, while the inner metal nitride diameter of only 5-20 nm. The tube/rod on graphene surface could be ascribed to carbon micro/nano tubes grown under the catalysis of transition metal core. TEM (Fig. 3) images show Fe_3N is uniformly distributed onto graphene layers with size of roughly 10-20 nm. TMN^{n+}-EN_x chelates has negatively charged–NH_2 groups which could adsorb to G-O sheets through electrostatic interaction with O-containing functional groups on G-O surface or by forming a O=C-NH bond with carboxyl groups. Therefore the uniform distribution of metal nitride on graphene sheets could be achieved, due to O-containing functional groups site from G-O leading to uniform adsorption and distribution of TMN^{n+}-EN_x chelates. The TEM images show the distribution of FeN in graphene is homogeneous, and some of FeN has carbon shell with thickness of 1~10 nm. The FeN/N-rG-O has lattice spacing of 0.21 ± 0.05 nm, corresponding to the (101) lattice planes of FeN, which is consistent with XRD result shown in Fig. 2. The graphitic shells with lattice spacing from 0.29-0.41 nm, is quite irregular, which is probably composed of N-doped graphene layers, or amorphous carbon from carbonization of G-O or/and EN molecules.

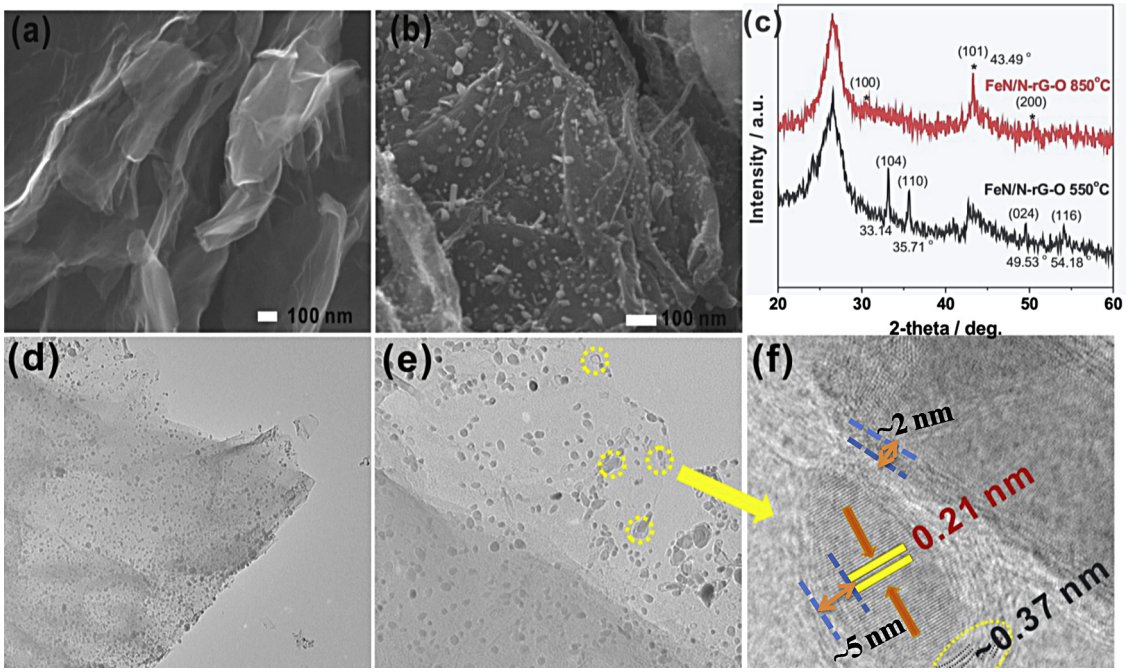

Fig. 2. SEM images of G-O (a) and FeN/N-rG-O 850 °C (b). XRD patterns (c) corresponding to FeN/N-rG-O samples prepared under annealing temperature of 850 and 550 °C respectively.TEM (d, e) and HRTEM (f) of FeN/N-rG-O 850 °C.

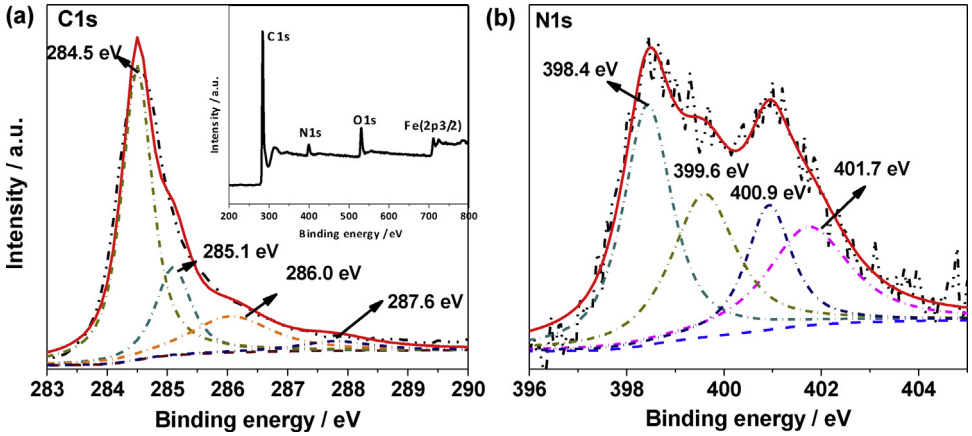

Fig. 3. C1s (a) and N1s (b) core-level XPS and survey scan of FeN/N-rG-O 850 °C (inset of a).

To confirm N-doping and N bonding states of graphene, X-ray photoemission spectroscopy (XPS) studies were carried out. The survey scan of FeN/N-rG-O showed the presence of N and O together with Fe. The N bonding states are identified by C1s and N1s spectra. The C1s peak of FeN/N-rG-O can be fitted with three different components with binding energy of 284.5, 285.1 and 286.0 eV, corresponding to sp^2 hybridized C atoms, C-N bond, and C-O bond, respectively. N1s spectrum of FeN/N-rG-O can also be deconvoluted into four components. The peak at 398.4 eV corresponding to "pyridinic" nitrogen, which contributes to π-conjugated system on graphene with a pair of π electrons. The peak centered at 399.6 eV could be assigned to "nitrile" nitrogen. [36] The peak at 401.7 eV indicates presence of "quaternary nitrogen", which is sp^2 hybridized N bonded with three sp^2 hybridized C neighbors. The peaks at 400.9 eV can be ascribed to "pyrrole-like" nitrogen where N incorporated in five-membered heterocyclic ring. The N in the composite is predominantly present in form of pyridinic and nitrile nitrogen. The percentage of N in the form of nitrides to the total N content is 18.5%, corresponding to 1.3 at% or 9.3 wt% metal nitride species in the FeN/N-rG-O 850 °C sample, which agrees well with the result obtained from inductively coupled plasma-optical emission spectrometer analysis (12.5 ± 2.0wt% of FeN).

3.2. Electrochemical Characterization and Discussion

The lithium insertion/de-insertion properties in FeN/N-rG-O are shown in Fig. 4a. Cyclic voltammogram of FeN/N-rG-O conducted at a scan rate of 1 mV s^{-1} in 1 M solution of $LiPF_6$ in 1:1 (v:v) mixture of EC and DMC as electrolyte against Li metal as counter and reference electrode are shown in Fig. 4a. The first cycle had cathodic peak at 0.3 V and disappeared from the second cycle, which could be attributed to the decomposition of electrolyte and formation of solid electrolyte interface (SEI) layer. After the first cycle, peak around 0.8 V could be observed, corresponding to Li reversible reaction with FeN similar like previously reported metal nitrides. [17,37]

Fig. 4b shows the initial three discharge and charge curves of FeN/N-rG-O at a current density of 50 mA g^{-1} in the voltage window of 0.01- 3.0 V vs. Li^+/Li. During the first discharge, which is react with Li, the voltage drops from open circuit voltage (OCV ~ 3.0 V) continuously to ~ 0.85 V, then appears two broad plateaus around 0.75 and 0.35 V. After the first cycle discharge and charge, the discharge plateau of the cell is around 1.1~1.0 V and below 0.75 V range. The FeN/N-rG-O delivers 750 and 510 mAhg^{-1} capacities for the first discharge and charge, respectively. Therefore, the irreversible capacity loss for FeN/N-rG-O cell is 240 mAhg^{-1}, and the initial columbic efficiency is 68%. The third cycle shows minor difference compared with the second circle on curve shape, peak intensity and integral area, indicating the electrochemical reversibility of TMN-G is gradually built after the first cycle. The columbic efficiency of FeN/N-rG-O cell is 96 ± 2% after the first three cycles. With an increase in the cycle number, the reversible capacity increases from 665 mAhg^{-1} in the 2nd cycle to 698 mAhg^{-1} at the end of 50th cycle at a current density of 50 mA g^{-1} (Fig. 4c). The increase of capacity with cycle is interesting, but already reported as an electrochemical behavior for some other metal nitrides. [16] For rG-O material, the capacity retention after 100 cycles was only about 278 mAh g^{-1} and the irreversible capacity loss for rG-O during cycling are 959 mAh g^{-1}. The reversible capacity of N-rG-O decrease from 510 mAh/g to 400 mAh/g, higher than that of rG-O even after 100 cycles.(Fig. 4d). The CV curves of FeCoN/N-rG-O cell are shown in Fig. 5a, where a cathodic current density stabilize at the third cycle; indicating the SEI was built after the first cycle. The initial three discharge and charge curves of FeCoN/N-rG-O cell at a current density of 100 mA/g are shown in Fig. 5b. During the first discharge, the FeCoN/N-rG-O cell voltage drops continuously from 3.0 V to 0.75 V, and then appears two broad plateaus around 0.75 and below 0.60 V. The discharge profiles of the FeCoN/N-rG-O cell stabilized after 2nd cycle, and below 1.5 V discharge range gives >90% of the discharge capacity value. The discharge profile of FeCoN/N-rG-O cell is lower than previously reported Co_3O_4/rG–O, [38] indicating FeCoN is superior anode materials than Co_3O_4 in the aspect of discharge potential. For FeCoN/N-rG-O, the capacity is 815 mAh/g at the first cycle, and the reversible capacity is 495 mAh/g which gradually increase to 520 mAh/g after 60 cycles at a current density of 100 mA/g (Fig. 5c). For CoN/N-rG-O and NiN/N-rG-O, the general trend of cycling behavior is similar, which is the compensation of first few cycle capacity losses in the following tens or hundreds of cycles.

FeCoN/N-rG-O, NiN/N-rG-O, and CoN/N-rG-O shows metal nitride nanoparticles with crystal size of 1-2 nm distribute on the N-rG-O surface. The presence of N and Ni are confirmed by electron energy loss spectroscopy (EELS). The core-loss K-edge of C and N is located at 284 and 401 eV, while the L2.3 edge of nickel at 850 eV (Fig. S1). At current density of 50 mA g^{-1}, the capacity retention of NiN/N-rG-O, and CoN/N-rG-O are 730 and 667 mAh g^{-1} respectively (Fig. S2).

The rG-O has large amount of defects at edge sites and internal/basal plane (vacancies etc.), with nanodomains embedded planer space. Chemically derived graphene has abundant dangling bonds, defects, high oxygen content which has higher reactivity toward the electrolytes and easily result in decomposition of electrolyte in the first discharging process. Therefore, graphene electrodes have severe capacity loss during the first few cycles.

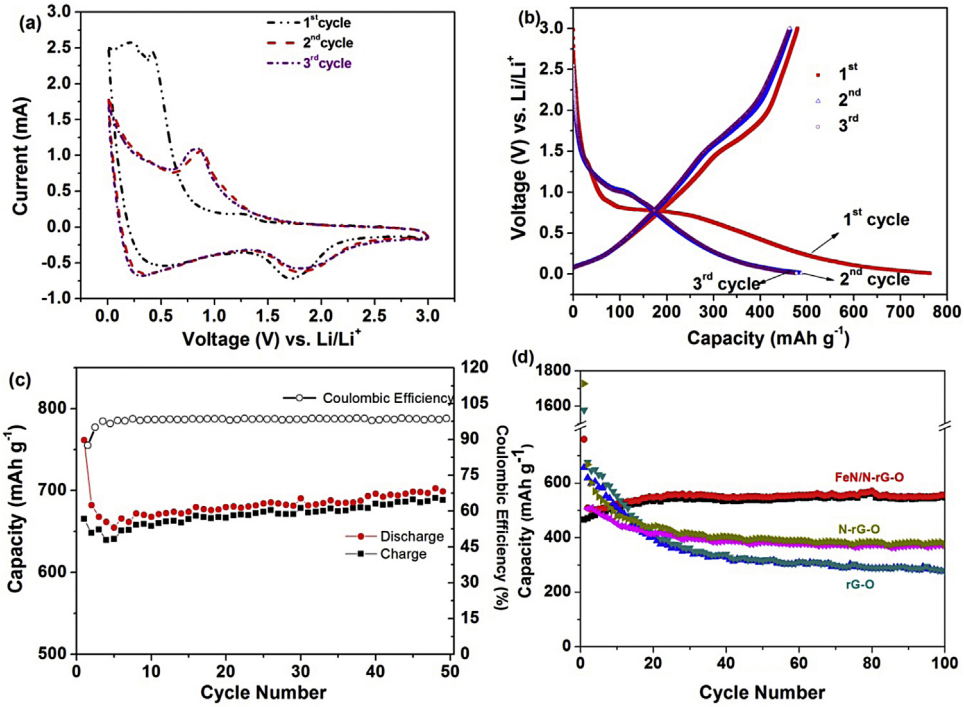

Fig. 4. Electrochemical characterizations of a half-cell composed of FeN/N-rG-O and Li. The specific capacities are calculated based on the mass of FeN/N-rG-O composite including binder and carbon black. (a) the first 3 cycles of CV curve under a current density of 1 mV s^{-1}; (b) first three charge and discharge curves of FeN/N-rG-O composite at a current density of 100 mA g^{-1}; (c) capacity retention of FeN/N-rG-O at current density of 50 mA g^{-1} for 50 cycles; and (d) the electrochemical capacity comparison of rG-O, N-rG-O and FeN/N-rG-O at current density of 100 mA g^{-1}.

[39,40] The heteroatoms doping for anodes, especially N is effective for Li ion battery capacity and cycle performance improvement. The reversible capacity of N doped graphene is two times larger than that of pristine graphene, [39] and N doped CNTs delivered a reversible capacity of 494 mAh g^{-1} *vs.* 260 $mAhg^{-1}$ for CNTs. [41] However, introducing of N to graphene also has shortcomings, such as large irreversible capacity loss in the initial cycle. [42] CNT grown from 100% acetonitrile with N content of 2.89 at.% has a first discharge capacity of 827 $mAhg^{-1}$, with irreversible capacity of 586 $mAhg^{-1}$, [43] and the initial columbic efficiency of N doped graphene is 32%. [39] The N might react with Li irreversibly *via* the following reaction:

$$3Li + N \rightarrow Li_3N \quad (1)$$

Lithium nitride, Li_3N, is stable binary alkali metal nitride and has a unique layered structure in which Li_2N layers are separated by layers of Li atoms. The transition metal oxides, such as Co_3O_4, Fe_2O_3, or NiO could reversibly react with Li as expressed in eq.(2). Upon oxidation, metal oxides react with Li_2O and reform metal oxide at voltages ranging from 1.5 to 2.5 V vs. Li/Li^+

$$M_xO_y + 2yLi + +2ye^- \leftrightarrow xM + yLi_2O \quad (2)$$

While, the reaction of binary nitrides behave as Li "sink". Reports indicate that the reaction of TM_xN_y with Li^+ consist of a conversion reaction of Me_xN_y form lithium metal alloys (LiMe) and β-Li_3N. [17,21,23] Further oxidation of LiTMN generated metal, while β-Li_3N contribute to the transformation into LiTMN (eq. 3). [15,17] N abundant LiTMN ($Li_{3-x}Fe_xN$ in eq.4), where Me is a transition

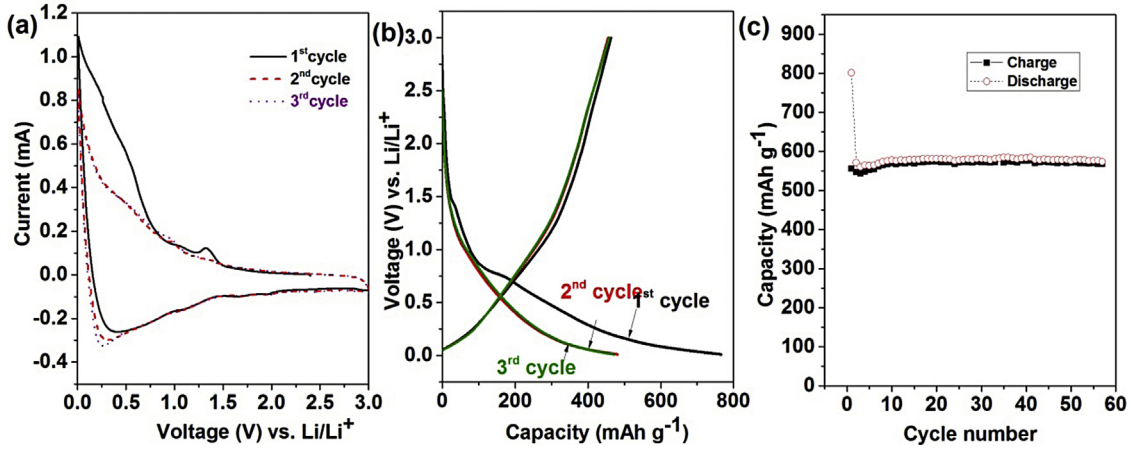

Fig. 5. Electrochemical characterizations of a half-cell composed of FeCoN/N-rG-O and Li. (a) the first 3 cycles of CV curve under a current density of 1 mV s^{-1}; (b) charge and discharge curves of FeCoN/N-rG-O composite for the first three cycles at a current density of 100 mA g^{-1}; (c) capacity retention of FeCoN/N-rG-O at current density of 100 mA g^{-1} for 60 cycles.

metal as Co, Ni, are isostructural to the hexagonal layered Li_3N. LiTMN would further react with Li and convert to metal and Li_3N (eq. 4). From eq. (3) to (5) as explored by previous researchers, TM_xN_y reacts with Li produce LiTMN, which is regarded as the most promising anode materials in recent years. [3,23,24] The 3d metals of Ni, Co, and Fe produced from eq. (3) could greatly enhance the electrochemical activity of Li-ion anode toward the formation/decomposition of Li_3N by reaction of metal nitride with lithium, as eq. (5) show. [17]

$$Fe_3N + xLi^+ \leftrightarrow Li_xFe_{3-x}N + xFe \quad (3)$$

$$Li_xFe_{3-x}N + 3\text{-}xLi \leftrightarrow 3\text{-}xFe + Li_3N \quad (4)$$

$$3Fe + Li_3N \leftrightarrow Fe_3N + 3Li \quad (5)$$

Therefore, CoN and FeN as anode produce metallic transition metal of Co or Fe (eq. 3), one part of metallic Fe or Co is nitrated and reduced in the lithium electrochemical reaction (eq. 4); another part of Co or Fe seems to act as an active spectator to help drive the formation and decomposition of Li_3N (eq. 5). The as proposed mechanism is in agreement with previous reports. [14,16]

As the specific capacity of nanophase is strongly dependent on lithium transport distance, [44] the reduction of TMN crystal size while introduce of electron conductive coating layer would be greatly helpful. In as-developed method, the N containing EN also introduced N doping to G-O, as determined by XPS results. The Li_3N generated during the first discharge could further be decomposed by metal to produce $LiTM_xN_y$ (eq. 3 and 4), which are proven to be capable of reacting with Li reversibly. [23] Therefore, after the 2nd cycle, there is no capacity decrease for all TMN/N-rG-O, in all as-prepared samples, such as FeN-rG-O FeCoN-rG-O, CoN-rG-O and NiN-rG-O. The N doping of graphene on the other hand, have improved the conductivity, which contribute to the fast charge separation, transportation, and further leading to large capacity and excellent cyclability.

4. Conclusions

Herein, we reported a universal strategy to synthesize the transition metal nitride nanoparticles anchored on conducting N-modified graphene as an advanced anode material for high-performance Li-ion battery. The TMN has size of 5-20 nm in size and homogeneously anchored on graphene sheets. The electrochemical properties of the TMN/N-rG-O composites results demonstrate the hybrid materials has high capacity (> 650 $mAhg^{-1}$) and excellent cyclability, low charge discharge window potential (<1.5 V vs. Li/Li^+). This method is applicable to prepare TMN/N-rG-O composites, such as FeN-rG-O FeCoN-rG-O, CoN-rG-O and NiN-rG-O. Due to the low-cost and simplified preparation method, these TMN/rG-O composites are promising for large-scale preparation, and industrial application.

Appendix A. Supplementary data

Supplementary data associated with this article can be found, in the online version, at http://dx.doi.org/10.1016/j.electacta.2014.04.073.

References

[1] A.S. Arico, P. Bruce, B. Scrosati, J.M. Tarascon, W. Van Schalkwijk, Nanostructured materials for advanced energy conversion and storage devices, Nat. Mater. 4 (2005) 366–377.
[2] B.E. Conway, Transition from supercapacitor to battery behavior in electrochemical energy-storage, J. Electrochem. Soc. 138 (1991) 1539–1548.
[3] J.M. Tarascon, M. Armand, Issues and challenges facing rechargeable lithium batteries, Nature 414 (2001) 359–367.
[4] Y.G. Li, B. Tan, Y.Y. Wu, Mesoporous CO3O4 nanowire arrays for lithium ion batteries with high capacity and rate capability, Nano Lett. 8 (2008) 265–270.
[5] X.W. Lou, D., Deng, J.Y., Lee, J., Feng, L.A. Archer, Self-supported formatnion of needlelike Co3O4 nanotubes and their application as lithium-ion battery electrodes, Adv. Mater., 20 (2008) 258-+.
[6] N.C. Li, C.R. Martin, A high-rate, high-capacity, nanostructured Sn-based anode prepared using sol-gel template synthesis, J. Electrochem. Soc. 148 (2001) A164–A170.
[7] S.M. Paek, E. Yoo, I. Honma, Enhanced Cyclic Performance and Lithium Storage Capacity of SnO(2)/Graphene Nanoporous Electrodes with Three-Dimensionally Delaminated Flexible Structure, Nano Lett. 9 (2009) 72–75.
[8] E. Kang, Y.S. Jung, A.S. Cavanagh, G.H. Kim, S.M. George, A.C. Dillon, J.K. Kim, J. Lee, Fe(3)O(4) Nanoparticles Confined in Mesocellular Carbon Foam for High Performance Anode Materials for Lithium-Ion Batteries, Adv. Funct. Mater. 21 (2011) 2430–2438.
[9] M.V. Reddy, T. Yu, C.H. Sow, Z.X. Shen, C.T. Lim, G.V.S. Rao, B.V.R. Chowdari, alpha-Fe2O3 nanoflakes as an anode material for Li-ion batteries, Adv. Funct. Mater. 17 (2007) 2792–2799.
[10] P. Poizot, S. Laruelle, S. Grugeon, L. Dupont, J.M. Tarascon, Nano-sized transition-metaloxides as negative-electrode materials for lithium-ion batteries, Nature 407 (2000) 496–499.
[11] Y. Idota, T. Kubota, A. Matsufuji, Y. Maekawa, T. Miyasaka, Tin-based amorphous oxide: A high-capacity lithium-ion-storage material, Science 276 (1997) 1395–1397.
[12] L. Baggetto, N.A.M. Verhaegh, R.A.H. Niessen, F. Roozeboom, J.C. Jumas, P.H.L. Notten, Tin Nitride Thin Films as Negative Electrode Material for Lithium-Ion Solid-State Batteries, J. Electrochem. Soc. 157 (2010) A340–A347.
[13] Q. Sun, Z.W. Fu, Vanadium nitride as a novel thin film anode material for rechargeable lithium batteries, Electrochim. Acta 54 (2008) 403–409.
[14] Q. Sun, Z.W. Fu, Mn3N2 as a novel negative electrode material for rechargeable lithium batteries, Appl. Surf. Sci. 258 (2012) 3197–3201.
[15] F. Gillot, J. Oro-Sole, M.R. Palacin, Nickel nitride as negative electrode material for lithium ion batteries, J. Mater. Chem. 21 (2011) 9997–10002.
[16] B. Das, M.V. Reddy, P. Malar, T. Osipowicz, G.V.S. Rao, B.V.R. Chowdari, Nanoflake CoN as a high capacity anode for Li-ion batteries, Solid State Ionics 180 (2009) 1061–1068.
[17] Z.W. Fu, Y. Wang, X.L. Yue, S.L. Zhao, Q.Z. Qin, Electrochemical reactions of lithium with transition metal nitride electrodes, J. Phys. Chem. B 108 (2004) 2236–2244.
[18] Q. Sun, Z.W. Fu, An anode material of CrN for lithium-ion batteries, Electrochemical and Solid State Letters 10 (2007) A189–A193.
[19] B. Das, M.V. Reddy, G.V.S. Rao, B.V.R. Chowdari, Synthesis and Li-storage behavior of CrN nanoparticles, Rsc Advances 2 (2012) 9022–9028.
[20] M. Nishijima, Y. Takeda, N. Imanishi, O. Yamamoto, M. Takano, Li Deintercalation and Structural-Change in the Lithium Transition-Metal Nitride Li3fen2, J. Solid State Chem. 113 (1994) 205–210.
[21] M. Nishijima, T. Kagohashi, M. Imanishi, Y. Takeda, O. Yamamoto, S. Kondo, Synthesis and electrochemical studies of a new anode material, Li3-xCoxN, Solid State Ionics 83 (1996) 107–111.
[22] L.H.D. S. H. Elder, F. J. DiSalvo, LiMoN2: The First Metallic Layered Nitride Chem. Mater., 4, 928-937.
[23] J.L.C. Rowsell, V. Pralong, L.F. Nazar, Layered lithium iron nitride: A promising anode material for Li-ion batteries, J. Am. Chem. Soc. 123 (2001) 8598–8599.
[24] Y. Takeda, M. Nishijima, M. Yamahata, K. Takeda, N. Imanishi, O. Yamamoto, Lithium secondary batteries using a lithium cobalt nitride, Li2.6Co0.4 N, as the anode, Solid State Ionics 130 (2000) 61–69.
[25] H. Asahara, T. Migita, T. Tanaka, K. Kawabata, Microstructure and electrical properties of CoNX thin films deposited by unbalanced magnetron sputtering, Vacuum 62 (2001) 293–296.
[26] I. Nakatani, T. Furubayashi, Iron-Nitride Magnetic Fluids Prepared by Plasma Cvd Technique and Their Magnetic-Properties, J. Magn. Magn. Mater. 85 (1990) 11–13.
[27] K. Oda, T. Yoshio, K. Oda, Preparation of Co-N Films by Rf-Sputtering, J. Mater. Sci. 22 (1987) 2729–2733.
[28] D.R. Dreyer, S. Park, C.W. Bielawski, R.S. Ruoff, The chemistry of graphene oxide, Chem. Soc. Rev. 39 (2010) 228–240.
[29] D. Chen, L.H. Tang, J.H. Li, Graphene-based materials in electrochemistry, Chem. Soc. Rev. 39 (2010) 3157–3180.
[30] G.X. Wang, B. Wang, X.L. Wang, J. Park, S.X. Dou, H. Ahn, K. Kim, Sn/graphene nanocomposite with 3D architecture for enhanced reversible lithium storage in lithium ion batteries, J. Mater. Chem. 19 (2009) 8378–8384.
[31] Y. Zhong, X. Wang, K. Jiang, J.Y. Zheng, Y. Guo, Y. Ma, J. Yao, A facile synthesis and lithium storage properties of Co3O4–C hybrid core-shell and hollow spheres, J. Mater. Chem. 21 (2011) 17998.
[32] X.J. Zhu, Y.W. Zhu, S. Murali, M.D. Stollers, R.S. Ruoff, Nanostructured Reduced Graphene Oxide/Fe(2)O(3) Composite As a High-Performance Anode Material for Lithium Ion Batteries, Acs Nano 5 (2011) 3333–3338.
[33] G.X. Wang, J. Yang, J. Park, X.L. Gou, B. Wang, H. Liu, J. Yao, Facile synthesis and characterization of graphene nanosheets, J. Phys. Chem. C 112 (2008) 8192–8195.
[34] V. Raghavan, C-Fe-N (carbon-iron-nitrogen), J. Phase Equilibria 14 (1993) 620–621.
[35] Y.W. Y. Ohshima, N., Tsubouchi, Y. Ohtsuka, Approach to the iron-catalyzed formation process of N2 from heterocyclic nitrogen in carbon by use of XRD and XPS methods, ACS Fuel 2000 (San Francisco), (2000).

[36] W. Ding, Z.D. Wei, S.G. Chen, X.Q. Qi, T. Yang, J.S. Hu, D. Wang, L.J. Wan, S.F. Alvi, L. Li, Space-Confinement-Induced Synthesis of Pyridinic- and Pyrrolic-Nitrogen-Doped Graphene for the Catalysis of Oxygen Reduction, Angew. Chem. Int. Edit. 52 (2013) 11755–11759.
[37] K.J. Zhang, H.B. Wang, X.Q. He, Z.H. Liu, L. Wang, L. Gu, H.X. Xu, P.X. Han, S.M. Dong, C.J. Zhang, J.H. Yao, G.L. Cui, L.Q. Chen, A hybrid material of vanadium nitride and nitrogen-doped graphene for lithium storage, J. Mater. Chem. 21 (2011) 11916–11922.
[38] H. Kim, D.H. Seo, S.W. Kim, J. Kim, K. Kang, Highly reversible Co3O4/graphene hybrid anode for lithium rechargeable batteries, Carbon 49 (2011) 326–332.
[39] A.L.M. Reddy, A. Srivastava, S.R. Gowda, H. Gullapalli, M. Dubey, P.M. Ajayan, Synthesis Of Nitrogen-Doped Graphene Films For Lithium Battery Application, Acs Nano 4 (2010) 6337–6342.
[40] Z.S. Wu, W.C. Ren, L. Xu, F. Li, H.M. Cheng, Doped Graphene Sheets As Anode Materials with Superhigh Rate and Large Capacity for Lithium Ion Batteries, Acs Nano 5 (2011) 5463–5471.
[41] J.L. Xifei Li, Yong Zhang, Yongliang Li, Hao Liu, Xiangbo Meng, Jinli Yang, Dongsheng Geng, Dongniu Wang, Ruying Li, Xueliang Sun, High concentration nitrogen doped carbon nanotube anodes with superior Li+ storage performance for lithium rechargeable battery application, J. Power Sources 197 (2012) 238–245.
[42] H. Kim, D.H. Seo, S.W. Kim, J. Kim, K. Kang, Highly reversible Co(3)O(4)/graphene hybrid anode for lithium rechargeable batteries, Carbon 49 (2011) 326–332.
[43] L.G. Bulusheva, A.V. Okotrub, A.G. Kurenya, H.K. Zhang, H.J. Zhang, X.H. Chen, H.H. Song, Electrochemical properties of nitrogen-doped carbon nanotube anode in Li-ion batteries, Carbon 49 (2011) 4013–4023.
[44] P. Tartaj, J.M. Amarilla, Iron oxide porous nanorods with different textural properties and surface composition Preparation, characterization and electrochemical lithium storage capabilities, J. Power Sources 196 (2011) 2164–2170.